Phase Composition and Structure of Nanocrystalline Films of NiCu, NiCo, and NiFe Alloys

V. B. Loboda, S. M. Khursenko, and V. O. Kravchenko

Abstract The work is devoted to the study of the crystal structure and phase composition of thin films of NiCu, NiCo, and NiFe alloys. Alloy films with thicknesses of 1–200 nm were obtained in vacuum at a residual gas pressure of ~10^{-4} Pa. The films were condensed at a rate of $\omega \geq 1$ nm/s. For electron microscopy studies, both NaCl chips and thin carbon layers were used as substrates. All films underwent stabilizing annealing in a vacuum to T = 700 K. In films based on NiCu and NiCo alloys with effective thicknesses of d < 10 nm, obtained on amorphous substrates at T = 300 K, an island structure was observed. In structurally continuous annealed films of NiCu and NiCo alloys at $C_{Co} < 70$ wt.%, an fcc structure was formed. For NiCu alloy films, depending on the concentration of the components, the crystal lattice parameter was a = 0.353–0.362 nm. Films of the NiCo alloy at $C_{Co} \geq 80$ wt.% had a two-phase composition (fcc + hcp)-solid solution NiCo. Films of the $Ni_{50}Fe_{50}$ alloy had a fcc lattice with a = 0.359–0.361 nm. Unannealed films exhibited a fine-grained structure; annealing led to an increase in grain size to 50 nm.

Keywords Thin films · NiCu alloy film · NiCo alloy film · NiFe alloy film · Crystal structure · Phase composition

The work is devoted to the study of the morphology, crystal structure, and phase composition of thin films of NiCu, NiCo, and NiFe alloys.

Films with thicknesses d = 1–200 nm were obtained in a vacuum at a residual gas pressure of ~10^{-4} Pa by the method of separate simultaneous evaporation of the components. For the evaporation of copper, a resistive heating method was used; for the evaporation of nickel, cobalt, and iron, an electron-beam method was used. The films condensed at a rate $\omega \geq 1$ nm/s. Both NaCl cleavages and thin layers of carbon were used as substrates for electron microscopic studies.

V. B. Loboda (✉) · S. M. Khursenko · V. O. Kravchenko
Sumy National Agrarian University, Sumy, Ukraine
e-mail: loboda-v@i.ua

A. D. Pogrebnjak et al. (eds.), *Nanocomposite and Nanocrystalline Materials and Coatings*, Advanced Structured Materials 214,
https://doi.org/10.1007/978-981-97-2667-7_8

The formation of the fcc NiCu alloy occurs directly during the condensation of the components in the entire thickness range; for structurally continuous annealed films, depending on the concentration of the components, the crystal lattice parameter is a = 0.353–0.362 nm in accordance with Vegard's rule. Unannealed and annealed films of the NiCo alloy at $C_{Co} < 70$ wt.% have an fcc structure; annealed films with $C_{Co} \geq 80$ wt.% have a two-phase composition (fcc + hcp)-solid solution NiCo. The change in the lattice parameter of fcc-NiCo films with increasing C_{Co} is described by Vegard's rule.

In films of NiCu and NiCo alloys with effective thicknesses d < 10 nm, obtained on amorphous substrates at T = 300 K, an island structure is observed.

$Ni_{50}Fe_{50}$ alloy films have an fcc lattice with a = 0.359–0.361 nm; unannealed films have a fine-grained structure; annealing leads to an increase in grain size up to 50 nm.

1 Introduction

The study of the physical properties of thin metal films is due both to obtaining results that contribute to the solution of a number of fundamental problems in solid-state physics and to the prospects for their practical application. The use of films has led to significant progress in microelectronics, high-frequency technology, optoelectronics, optics, and many other areas of modern science and technology.

A special place in the physics of thin films is occupied by films of magnetically ordered metals Ni, Fe, and Co. This is primarily due to the fact that their study allows solving a number of fundamental problems for «two-dimensional magnetism». In addition, in recent years, a number of new fundamental effects (giant magnetoresistance, spin-polarized tunneling, colossal magnetoresistance, etc.) have been discovered in film objects based on these metals, which form the basis for the development of miniature magnetoelectronic devices, new recording and storage methods information, and new types of highly sensitive sensors and transducers (nanoelectronics, spintronics).

Along with studies of films of pure metals (Ni, Cu, Co, Fe), it is promising to study films of metal alloys [1–6] and film multilayer structures [7–11], which include these metals. Alloy films (as well as bulk alloys) have a number of advantages over pure metal films: by changing the composition of the alloy, materials with other electrophysical, physicochemical, and operational properties can be obtained. Along with traditional film objects, in recent decades, a scientific direction has been formed related to the improvement of the service properties of massive metal samples by methods of creating layered structures in modified near-surface layers [12–14].

The properties of thin films, as a rule, differ significantly from the properties of bulk samples. Limiting the size of film objects in one of the directions leads to the appearance of so-called size effects, which are weakly expressed or not observed at all in the massive state. In the early stages of formation, thin films are not continuous. They are formed from small islands that may (or may not) be physically connected to

each other depending on the thickness of the layer. The physical properties of island films differ significantly from the properties of both bulk metals and solid metal films. This paper presents the results of studying the morphology, crystal structure, and phase composition of NiCu, NiCo, and NiFe alloy films.

2 Technique and Methodology of Experiments

2.1 Preparation of Samples of Alloy Films

The method of obtaining metallic films by evaporation of the initial metal and its condensation in a vacuum (see, for example, [15]) has been widely used for many years in various fields of science and technology due to the universality of the technology, high productivity of the process, low energy consumption, absence of environmental pollution, etc. These and a number of other indicators determine the competitiveness of this method in comparison with other methods of film production (electrodeposition, cladding, metallization, sputtering, etc.). The quality of the formed films, the reproducibility of their functional properties, and the stability of characteristics under different operating conditions significantly depend on the patterns of evaporation and condensation.

To obtain thin alloy films, two main groups of methods are used: (1) the formation of multicomponent films directly on the substrate (separate evaporation of the components and subsequent diffusion annealing of multilayer structures, saturation in vapors); (2) the use of finished alloys as the initial metallizer (evaporation of the final portions of the alloy, stationary mode of evaporation, explosive evaporation).

Direct evaporation of compounds is quite widely used in the technology of obtaining multicomponent films and coatings due to its simplicity from the point of view of a constructive solution. At the same time, with this method of evaporation of alloys, the nature of the formation of films and their properties are determined by the fractionation of alloys during their evaporation, which leads to a discrepancy between the composition of the alloy film and the original alloy.

Some of the alloy films were obtained by us by the method of simultaneous condensation of the initial materials (Ni and Cu; Ni and Co) during their evaporation from two independent evaporators, which made it possible to directly obtain alloy films of arbitrary composition on the substrate.

To obtain part of NiCo film alloys, the method of evaporation of alloys of a given composition was also used. In doing so, the following considerations were taken into account. Data on «liquid–solid» phase equilibrium in bulk NiCo alloys [16, 17] show that the liquidus and solidus lines in this system practically coincide for any component concentration. As a result, no change in the chemical composition during melting can be expected. The difference between the vapor pressure of the Ni and Co metals at high temperatures is also insignificant, which also contributes

to maintaining the composition of the alloy films in accordance with the initial composition.

The choice of methods for the evaporation of metal components of alloy films was also determined by such physical properties of materials as the melting temperature and saturated vapor pressure. Thus, during the condensation of copper (films of NiCu alloys), the method of thermal evaporation of Cu was used. In this case, 0.05 mm thick tungsten foil ribbons were used as evaporators. Films of Ni, Co, NiFe alloys and parts of NiCo alloys were obtained by electron-beam evaporation of the initial metals using an electron diode gun. It consists of anode and cathode units, mechanically connected by ceramic insulator rods. A high voltage of up to 3 kV was applied to the gun anode. A small piece of the original metal (nickel, cobalt, NiCo, or NiFe alloys) was attached to the tungsten anode by spot welding. The anode was heated to the required temperature by bombarding it with a defocused beam of electrons evaporating from a hot cathode (tungsten wire 0.3 mm in diameter). The purity of the evaporated metals was no less than 99.98%.

The initial material for some films of NiCo alloys was specially prepared by us with small weighed portions of NiCo alloys of the required composition. For the preparation of weighed portions of these alloys, pure (no worse than 99.9%) Ni and Co metals were used. The concentration of the components was varied by changing the mass ratios of metals (the relative error in determining the mass is no more than 5%). Samples were prepared by melting samples of starting materials in a ceramic crucible under high vacuum conditions with exposure for 1 h at a temperature close to the melting temperature for homogenization. The weight loss did not exceed 1–2%.

Massive weights of an alloy known as permalloy 50N (composition: 49.5–50.0% Ni, impurities (Si, Mn) < 1%, the rest Fe [18]) were the material for the manufacture of NiFe films.

A VUP-5 M industrial vacuum unit was used to condense thin films. The pressure of the gases of the residual atmosphere in the process of obtaining samples was 10^{-3}–10^{-4} Pa.

Condensation of alloy films carried out on a substrate holder developed by us is shown in Fig. 1. Its design made it possible to obtain four film samples of practically the same thickness but different compositions in one technological cycle of deposition, both for measuring the electrophysical and magnetoresistive properties (3) and for studying the structure (5). The geometrical dimensions of the studied samples (a, b) were set by special masks made with high precision from nichrome foil.

The films were condensed at room temperature (300 K) of the substrate. The rate of condensation was determined experimentally from the deposition time and final sample thickness. During the condensation process, it was maintained constant and amounted to 0.5–1.5 nm/s, depending on the evaporation modes. The alloy films were condensed in the absence of an external orienting magnetic field (if the Earth's magnetic field was ignored), which made it possible to obtain magnetically isotropic films.

Depending on the type of research, two types of substrates were used (Fig. 1). To study the electrophysical and magnetoresistive properties, polished optical glasses (6) were used as substrates. Previously, contact copper pads (2) with a chromium sublayer

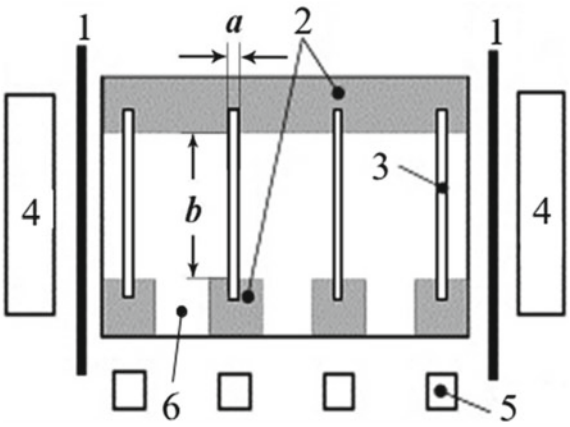

Fig. 1 Scheme of a substrate holder with substrates for condensation of film alloys: 1—screens; 2—contact pads; 3—film samples (a = 2 ± 0.05 mm, b = 10 ± 0.05 mm); 4—glasses «witnesses»; 5—single crystals of NaCl or carbon films; 6—glass substrate

were applied to them to improve the adhesion of copper to glass. For structural studies, single crystals of NaCl (orienting substrate) and carbon films (amorphous substrate) were used as substrates (5). In addition, glass plates «witnesses» (4) were fixed on the substrate holder to measure the thickness. The screens (1) ensured that the components of the alloys were hit separately on the «witness» plates.

The film thickness was measured using an MII-4 microinterferometer with a laser light source (miniature semiconductor laser, $\lambda = 647$ nm). The interference pattern was recorded using a digital camera with data transferred to a computer for subsequent recording and processing. With this method, it is possible to reduce the error in measuring the film thickness, especially in the thickness range $d < 50$ nm. The film thickness measurement error is 5–10% for thicknesses 50–200 nm and 10–15% for thicknesses $d < 50$ nm.

It should be noted that, in the case of ultrathin ($d < 10$ nm) films, the film thickness is commonly understood as the weight film thickness, which is determined from the deposition time and the known deposition rate. In this case, it is customary to speak of the effective film thickness (see, for example, [19]). The process of condensation of the «witness» films was 100–150 s, and their thickness was 100 nm or more. This made it possible to measure their thickness with an accuracy of 5–10%. Taking into account the error in measuring the condensation time t_c, the error in determining the effective thickness is 55–60% at $t_c = 1$ s (for ultrathin films) and decreases to 10–15% with an increase in t_c more than 10 s.

To calculate the concentration of the alloy film components during separate condensation of the components, a method was used, the essence of which is illustrated by the diagram, shown in Fig. 2.

Based on the geometry of the «substrate-evaporator» system, the thickness of individual components at point M can be calculated from the relations [15]:

$$d_1 = d_{01}\left[1 + \left(\frac{l_1}{h}\right)^2\right]^{-\frac{3}{2}} \text{ and } d_2 = d_{02}\left[1 + \left(\frac{l_2}{h}\right)^2\right]^{-\frac{3}{2}}, \quad (1)$$

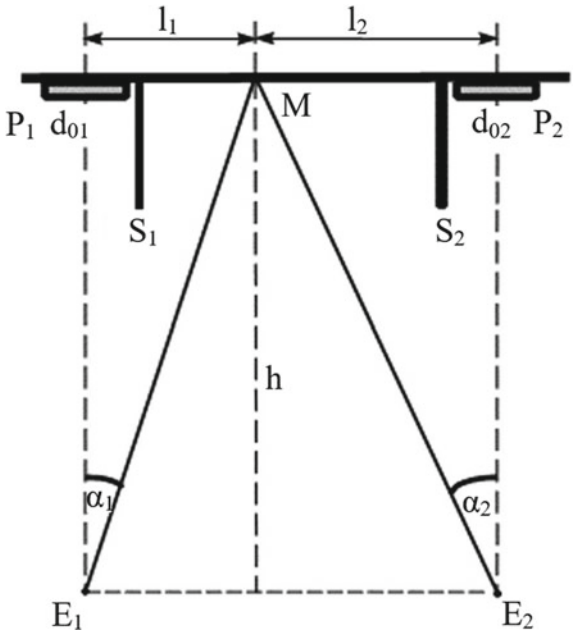

Fig. 2 Geometry of the «substrate-evaporators» system for calculating the concentration of the alloy components: S1, S2—screens; E1, E2—evaporators; P1, P2—glass plates «witnesses» of thickness

where d_0 is the film thickness at the point above the evaporator; d_{01}, d_{02} arethe thicknesses of the «witness» films; l_1, l_2 is the distance from the middle of the «witness» to the point M; h isthe distance from the plane of the evaporators to the plane of the substrate.

To find the concentration of the alloy film components at point M, one can use the obvious relations:

$$C_1 = \frac{D_1 d_1 \mu_1^{-1}}{D_1 d_1 \mu_1^{-1} + D_2 d_2 \mu_2^{-1}} \text{ and } C_2 = \frac{D_2 d_2 \mu_2^{-1}}{D_1 d_1 \mu_1^{-1} + D_2 d_2 \mu_2^{-1}}, \tag{2}$$

where D_1 and D_2 are the film densities of each of the materials; μ_1 and μ_2 are the molar masses of evaporated metals.

Taking into account that in bulk samples $D_{Ni} \approx D_{Cu} \approx D_{Co}$ and assuming that the same is true for films, relations (2) are transformed to the form:

$$C_1 = \frac{d_1 \mu_2}{d_1 \mu_2 + d_2 \mu_1} \text{ and } C_2 = \frac{d_2 \mu_1}{d_1 \mu_2 + d_2 \mu_1}. \tag{2a}$$

Since the concentration of the alloy film components was determined by the thicknesses d_1 and d_2, the error in determining the concentration of the components is the same as for the thickness.

2.2 Study of the Structure and Phase Composition of Films

To study the crystal structure and phase composition of film samples, electron microscopy (transmission electron microscopes EM-125, PEM-100-01) and electron diffraction (electronograph) studies were carried out. To carry out these studies, the films were condensed both on fresh (001) NaCl or KBr cleavages (single-crystal orienting substrates) and on carbon films (amorphous substrates). Carbon films simulated the conditions of deposition of film samples on amorphous glass.

To obtain information about the size and shape of crystallites, the data of microimages of the crystal structure of film samples were statistically processed, from which the size of individual Li grains was determined. The obtained data were used to construct a grouped frequency distribution and a histogram in the form of the dependence N = f(L). The average size of crystallites in the film plane was determined using the relation:

$$L = \frac{N_1 L_1 + N_2 L_2 + \ldots + N_n L_n}{N_1 + N_2 + \ldots + N_n}, \quad (3)$$

where N_n and L_n are, respectively, the number and average size of crystallites for the n-th interval.

To determine the sizes of crystallites along the normal to the substrate surface (crystallite heights), we used the method of analyzing the profiles of diffraction lines on electron diffraction patterns, similar to the method used in X-ray diffraction analysis to determine the sizes of coherent scattering regions during X-ray diffraction in bulk materials.

3 Physical Properties of Co, Ni, Cu, Fe and Their Alloys in the Bulk State [16– 22]

Bulk **nickel** has an fcc lattice (Fm3m) over the entire temperature range with the parameter a = 0.35243 nm.

Bulk **copper** has an fcc lattice (Fm3m) over the entire temperature range with a = 0.36148 nm.

Cobalt in the bulk state has two polymorphic modifications (low-temperature α-phase and high-temperature β-phase). The low-temperature α-phase has a hexagonal close-packed (hcp) lattice (structural type A3, space group $P6_3/mmc$) with parameters a = 0.2507 nm, c = 0.40686 nm (at 273 K). The high-temperature β-phase, which is stable up to the melting temperature of the metal, has a face-centered cubic (fcc) lattice (structural type A1, space group Fm3m, a = 0.3548 nm). The temperature at the beginning of the transition of α-Co to β-Co is 750 K; the temperature at the beginning of the reverse transition is 676 K.

Iron in a massive state crystallizes in four polymorphic modifications. The α-Fe modification has a body-centered cubic (bcc) lattice (structural type A2, space group Im3m) with parameter a = 0.286653 nm. At a temperature of 1042 K (Curie temperature), a transition occurs to the β-phase with the same structural type, but with the parameter a = 0.2895 nm. In the temperature range 1184–1665 K, γ-Fe is formed with an fcc lattice (a = 0.36468 nm); at higher temperatures, the δ-phase with the bcc structure and with the parameter a = 0.29322 nm is stable.

Nickel with Fe, Co, Cr, Cu, Mn, Mo, W, and other elements of the periodic system forms substitutional solid solutions with an fcc lattice in a wide range of concentrations. Such alloys are characterized by high ductility and strength, obtained as a result of a decrease in the energy of stacking faults, a decrease in the diffusion mobility of atoms, and a change in the electronic structure upon alloying. Nickel alloys are distinguished by high emission properties, increased mechanical strength and corrosion resistance, and can be processed in all types of machining. Nickel and copper in the entire range of component concentrations (from 0 to 100%) form a solid solution and have a diagram with unlimited solubility of the components in the solid and liquid states (Fig. 3). The solid phase of the massive NiCu alloy has an fcc lattice with a parameter from $a_0 = 0.35243$ nm to $a_0 = 0.36148$ nm depending on the concentration of the components, in accordance with Vegard's rule. The Curie temperature θ_{0C} of NiCu alloys is less than θ_{0C} for Ni and lies above room temperature at $C_{Cu} < 33\%$, approaching 70 K at $C_{Cu} = 50$–55%.

NiCo alloys (Fig. 4) form predominantly substitutional solid solutions with a single-phase composition based on lattices of pure metals. At room temperature, alloys with a Co content of up to 65–67 at.% have an fcc lattice over the entire temperature range of the solid state.

For $C_{Co} > 75$ at.%, a solid solution with an hcp lattice (low-temperature α-phase) is characteristic; with an increase in temperature, an fcc lattice (β-phase) is formed (the hcp → fcc transition temperature depends on the concentration of the components). In this case, due to the fact that both phases are close-packed, there is a crystallographic size-orientational relationship between them. In the intermediate range of concentrations, we have a two-phase composition.

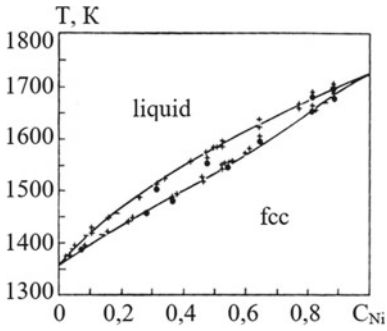

Fig. 3 Phase diagram of the state of the NiCu alloy

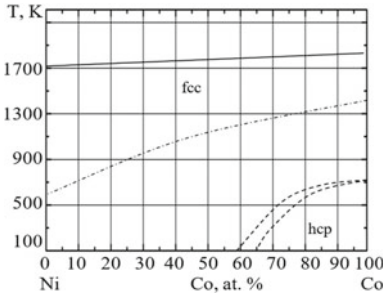

Fig. 4 Phase diagram of the state of the NiCo alloy

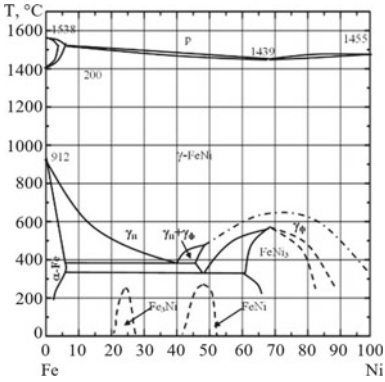

Fig. 5 Phase diagram of the state of the NiFe alloy

The phase composition of NiFe alloys (Fig. 5) is quite complex. Without going into a complete analysis of the phase diagram of this system, we note that we studied films obtained by evaporation of an alloy known as permalloy 50H (composition: 49.5–50.0% Ni, impurities (Si, Mn) < 1%, the rest Fe).

The alloy has high magnetic permeability, low coercive force (soft magnetic), almost zero magnetostriction, and significant (up to 5%) magnetoresistive effect. This alloy is characterized by an fcc lattice (Fm3m) with a = 0.359 nm.

4 Structure and Phase Composition of Ni, Co, Fe, and Cu Films

4.1 Growth Processes of Thin Metal Films

The physical properties of thin metal films largely depend on their structure, which, in turn, is determined by temperature, the state of the substrate, the vacuum conditions of

condensation, the deposition rate, and so on. Summarizing the experimental results, we can distinguish four main stages of film growth [15]:

– formation of critical nuclei and islands;
– growth of islands due to coalescence;
– formation of a mesh structure with narrow channels;
– formation of a structurally integral film.

The first stage of film formation is the collision of a vapor atom with a substrate. As a result of such a collision, the atom transfers part of its energy to the substrate and can then either re-evaporate or remain on the substrate. If the substrate temperature is high enough, then in the process of surface diffusion, the adsorbed atom can join an already existing group (cluster) of other atoms. In turn, such complexes of atoms are thermodynamically unstable (due to high surface energy) and can decompose. At the same time, due to the addition of new atoms, such a cluster can grow and reach a critical size, above which it becomes thermodynamically stable. As a result, such a cluster can become the nucleus of an island of a metal film.

Theoretical calculations show that the size of the critical nucleus for metals with a higher boiling point is smaller than for metals with a lower boiling point. For metals with high boiling points (particularly Fe, Ni, and Co), even small nuclei are thermodynamically stable. In addition, the size of the critical nucleus is affected by the surface energy of the metal and the substrate, the substrate temperature, and the rate of condensation.

The substrate temperature T_s is one of the main factors determining the film condensation mechanism [23, 24]. At temperatures below a certain Q_1 value inherent in a given material, the «saturated vapor-crystal» (SV-C) mechanism is realized. At $T_s > Q_1$, condensation is carried out according to the scheme «saturated vapor–liquid-crystal» (SV-L-C). Numerous experimental studies show that the temperature Q_1 is approximately $2/3T_m$ (where T_m is the melting temperature of the film material). The existence of another mechanism «saturated vapor-supercooled liquid-amorphous phase» was also experimentally confirmed, according to which a film is formed at a temperature below $Q_2 = 1/3T_m$.

With further condensation of the film, the process of island coalescence begins, which leads both to an increase in their size and to an increase in the free surface on which the formation of secondary islands begins. The film is a mesh structure in the form of islands separated by channels. Continued condensation and the formation of secondary islands eventually lead to the filling of the channels and the formation of a continuous film.

On neutral substrates, molecular beam condensation occurs only under the condition $T_s < T_c$ (T_s is the substrate temperature, T_c is the critical condensation temperature). In this case, depending on the rate of condensation ω, the temperature T_c can be either lower than the melting temperature of bulk samples T_m or higher. In

accordance with modern ideas about the mechanisms of formation of thin films in the literature (see, for example, [24–26]), it is customary to single out the following regimes of condensate growth:

(1) layer-by-layer (Frank-Van der Merwe regime) is realized if the atoms of the substance are connected with the atoms of the substrate (as a rule, single-crystal, with a close lattice parameter) stronger than one with the other; in this case, on the substrate, the construction of a monolayer of a substance is first completely completed, on which another monolayer, a third, etc., appears;
(2) island (Volmer-Weber mechanism) is realized in the case when the atoms of the substance are bound to each other more strongly than with the atoms of the substrate (usually neutral). In this case, small nuclei are formed on the surface of the substrate, which, as they grow, turn into large islands of the condensed phase. When the critical thickness is reached (determined by the kinetics of the condensation process), contacts appear between individual islands (a characteristic labyrinth structure with channels is formed). After the channels are filled, a continuous film is formed;
(3) intermediate (the Stranski–Krastanov regime), in which layer-by-layer condensation occurs first (1–2 layers are filled), after which the island growth regime begins. The main reason for changing the growth mechanisms is the change in the lattice parameter when the next layer is filled, which leads to a violation of the conditions for implementing the layer-by-layer growth mechanism and ensures the fulfillment of the island growth criterion.

A characteristic feature of the structure of thin films is the possibility of manifestation of the phase size effect in them [26]. In particular, in metal films, the appearance of new phases, which are not characteristic of a metal in the bulk state, and a decrease in the phase transition temperature in metal films, which have high-temperature phases, are possible. In island films, a change in the lattice parameter with thickness can also be observed; however, data on this effect are currently rather contradictory [24] (both an increase [26] and a decrease in the lattice parameter [19] were experimentally observed).

4.2 Phase Composition and Crystal Structure of Ni, Co, Fe, and Cu Films

A large number of experimental works have been devoted to the study of the crystal structure and phase composition of thin films of transition metals (for a detailed analysis, see, for example, [27]). Summarizing the experimental data, we can say that the structure and phase composition of transition metal films condensed in a vacuum quite definitely depend on a number of parameters: purity, microrelief and substrate temperature, substance deposition rate, the thickness of the condensed layer, subsequent thermal treatment of film samples, degree of vacuum, composition of the residual atmosphere, etc.

The fundamental influence on the phase composition and electrophysical properties of the films is the influence of such parameters as the pressure and composition of the gases of the residual atmosphere (P), the condensation rate (ω), and the substrate temperature (T_s). To describe the influence of these factors, we proposed an empirical condensation parameter α, which can be represented as follows:

$$\alpha = \frac{P}{\omega\sqrt{T_s}}$$

Analyzing numerous data as a whole, we can conclude that purer samples (without impurity phases) can be obtained by increasing the rate of their condensation (at P = const) or by decreasing the pressure of gases of the residual atmosphere P (at ω = const). Thus, at low values of α (low residual pressure or high rate of metal condensation), the best vacuum conditions will be realized. Then, in film samples, the phase corresponding to bulk samples should form with a higher probability. Conversely, at large values of α, the formation of impurity phases is possible.

Ni films [27]. It has been established that Ni does not have polymorphic modifications in films. In nickel films condensed under good vacuum conditions (for small values of the parameter α), only the fcc phase with the lattice parameter a = 0.351 ± 0.001 nm is observed.

The lattice parameters of pure Ni films almost coincide with the lattice parameters of bulk metal. The difference between the parameters is noted only in the case of ultrathin films. In this case, in films, depending on the conditions of production (primarily vacuum), the lattice parameter can either increase or decrease. When minimizing the influence of gaseous impurities, the lattice parameter only decreases with decreasing particle size. The reason for this decrease is usually associated with an increase in the concentration of vacancies in films compared to bulk samples.

Co films [27]. Studies of thin Co films have shown that, upon condensation on carbon substrates, either a low-temperature hcp phase or a high-temperature fcc phase is observed, depending on the particle size (film thickness) and substrate temperature. In the samples obtained on (001) NaCl, a two-phase fcc + hcp compound was observed both in island and continuous films. The phase composition in this case does not depend on the thickness and production conditions, but is completely determined by the size of the crystallites.

During the condensation of thin films in a high vacuum, a number of anomalous phases can form as a result of interaction with residual gases. Under ultrahigh vacuum conditions, anomalous phases are not observed. With a small value of the parameter α, and under high vacuum conditions, it is possible to obtain films with a crystalline structure of the corresponding bulk samples with a sufficiently high reproducibility.

Fe films [27]. Electron diffraction and X-ray diffraction studies of Fe films deposited on different substrates show that the films have a bcc lattice with a = 0.287 ± 0.001 nm. There is a large dispersion of the elements of the substructure and polyblockity in thickness even at thicknesses of 20–50 nm. This is due to the relatively high melting point of iron. As a consequence, condensation at room temperature is characterized by a significant degree of supercooling and a low diffuse mobility of

atoms. It should be added to this that in films of refractory metals, a small size of critical nuclei is observed, as a result of which a large number of crystals simultaneously grow in the film.

A change in the substrate temperature leads to a noticeable increase in the size of the crystallites. In particular, as the temperature rises from 300 to 720 K, the grain size in iron films 40 nm thick increases from 5 to 50 nm. The annealing of the films in vacuum also leads to a similar increase.

Cu films [27]. According to the research results, Cu films have an fcc lattice with a = 0.359–0.367 nm. At low condensation rates, a two-phase composition of fcc-Cu + fcc-Cu_2O films is also observed.

The increase in the lattice parameter of both unannealed and annealed in a vacuum chamber at 700 K copper films is explained by the dissolution of gases of the residual atmosphere (primarily oxygen) in Cu films, which is confirmed by mass spectrometric studies.

4.3 Phase Composition and Crystal Structure of the Alloy Films

In most cases, the structure of alloy films does not fundamentally differ from the structure of bulk analogues. However, as an analysis of the literature data shows, there may be some differences associated with the features of the films, in particular, with the manifestations of the phase size effect (PSE).

The structure and phase composition of alloys based on Ni, Fe, Co, and Cu in the film state are studied in a large number of experimental works (see, for example, the list of references in [27]), which, as a rule, are narrowly focused.

It is noted that for NiFe alloys, the single-phase region of the α-phase based on the bcc iron lattice increases compared to bulk alloys (up to 50% Ni), the reason for this is explained on the basis of PSE concepts. On the whole, the nature of the $\alpha \rightarrow \gamma$ transition curve is similar to the diagram obtained for annealing nonequilibrium bulk samples. For the NiFe alloy, at the initial stages of condensation, the formation of an amorphous structure is observed, which, upon further deposition, crystallized into the α phase.

In films of the $Ni_{50}Fe_{50}$ alloy, as in the bulk state, the formation of an fcc phase is most probable.

Structural and phase studies of $Ni_{50}Fe_{50}$ film alloys obtained by electron-beam evaporation of the initial alloy in vacuum at room temperature were carried out in [28]. The samples condensed at a rate of 0.5–1 nm/s. It was found that the $Ni_{50}Fe_{50}$ films are finely dispersed even after annealing them up to 700 K (the grain sizes of the annealed samples do not exceed 25 nm). For films with thicknesses of 16–160 nm, an fcc phase was observed with a lattice parameter a = 0.359–0.361 nm, which slightly exceeds the parameter of the initial bulk material (a_0 = 0.3586 nm [29]).

Films of NiCo alloys are characterized by a multiphase composition (a mixture of bcc, fcc, and hcp phases). Depending on the composition, one can observe an fcc or hcp phase, while the region of existence of hcp-NiCo can expand due to the phase size effect. Some differences between the phase diagrams of bulk and film samples are associated with the nonequilibrium of vacuum condensates.

5 Research Results

5.1 Films of NiCu Alloys

The films of NiCu alloys obtained by us in the range of thicknesses d = 1–200 nm and concentrations $0 < C_{Cu} < 100$ at .% have an fcc lattice with a parameter that depends on the concentration of the components and varies from a = 0.352 nm to a = 0.362 nm (for bulk alloys $0.3524 < a_0 < 0.3615$ nm [20]). The formation of the fcc alloy occurs already at the stage of condensation, which is confirmed by electron diffraction (Fig. 6). For all unannealed NiCu films, the first line (111) is very broad, but not double (this would take place in the case of the eutectic structure of the fcc-Ni + fcc-Cu alloy), since the difference $\Delta d_{111} = d_{111}(Cu)–d_{111}(Ni) = 0.009$ nm is quite sufficient for separate electron diffraction observation of the (111) Ni and (111) Cu lines. Electron diffraction patterns from thermally stabilized structurally continuous samples (Fig. 6d) sometimes show additional extremely thin lines (from 2 to 5 lines) of Cu_2O oxide, which has an fcc lattice with a = 0.424–0.450 nm. The most intense lines (111) Cu_2O and (220) Cu_2O are observed in electron diffraction patterns and from freshly condensed films at their condensation rate $\omega < 0.5$ nm/s. Lines of unstable oxide NiO or stable nitride Ni_3N were not recorded, although a number of authors (see, for example, [30]) noted this phase formation in nickel films.

In films of NiCu alloys, the values of the lattice parameter are somewhat higher compared to bulk samples (Fig. 7), which can be partly explained by the penetration of atoms from the residual atmosphere into the crystal lattice of the alloy, and partly by the fact that the atoms of one of the alloy components during the condensation process can occupy positions, which do not correspond to an ordered alloy.

For ultrathin samples of the NiCu alloy with effective thicknesses d = 1–7 nm, the crystal lattice parameter is 0.002–0.003 nm smaller compared to bulk samples. In experimental works [19, 24, 25, 31, 32], devoted to the study of ultrathin films of fcc metals, it was shown that, depending on the conditions of preparation, the lattice parameter can be either smaller or larger compared to the lattice parameter of bulk metal, increasing or decreasing with increasing island size. However, under conditions where the influence of gas impurities is minimized [24], the lattice parameter always decreases with decreasing particle size. The reason for this is either the presence of an additional (Laplace) pressure arising due to the small radius of curvature of the nanoparticle [19] or an increased (compared with the macroscopic sample) concentration of surface and near-surface vacancies in nanoparticles [24].

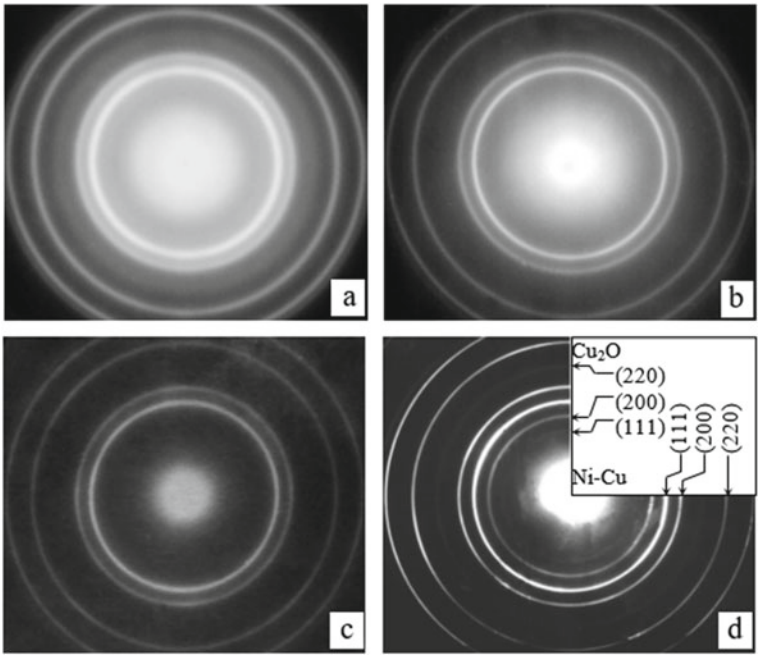

Fig. 6 Electron diffraction images of unannealed (**a**, **c**) and annealed to 700 K (**b**, **d**) NiCu alloy films: d ≈ 1 nm, C_{Cu} = 50.3 at.% (**a**, **b**); d = 40 nm, C_{Cu} = 38 at.% (**c**, **d**)

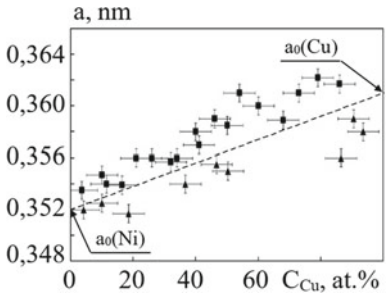

Fig. 7 Concentration dependence of the fcc lattice parameter of NiCu alloys (measurement temperature T = 300 K): ■—continuous films; ▲—island films; –·–·—Vegard's rule

Ultrathin Films of NiCu Alloys

For ultrathin films of NiCu alloys (Fig. 8), an island growth mode is realized. In this case, in freshly condensed ultrathin films of NiCu alloys with an effective thickness d ≈ 1–2 nm, regardless of composition, almost the same structure was observed with an average size of individual islands 1.5–2 nm. When the effective thickness d ≈ 3 nm is reached, which, in all likelihood, is critical for NiCu film alloys, the so-called classical labyrinth structure [32] with irregularly shaped islands connected to each other and channels between the islands approximately the same width. A further

increase in the effective thickness of the films to d ≈ 10 nm structurally manifested itself only in an increase in the density of islands and a decrease in the number of channels due to their gradual filling.

Since the condensation of film samples of the NiCu alloy was carried out on a neutral amorphous substrate (carbon film) at a temperature $T_s \approx 300$ K, less than $0.4T_m$ (T_m is the melting point of the alloy of a given concentration, 1400 K < T_m < 1700 K [16]), and diffusion the mobility of atoms in the islands was hindered, it can be assumed that the condensation of the alloys, in all probability, was carried out according to the «vapor → crystal» mechanism.

Subsequent annealing of the NiCu film alloys to T = 700 K leads to a significantly different morphological state of the samples, depending on their effective thickness. Thus, at d ≈ 1–3 nm, the islands are simply enlarged due to migration coalescence;

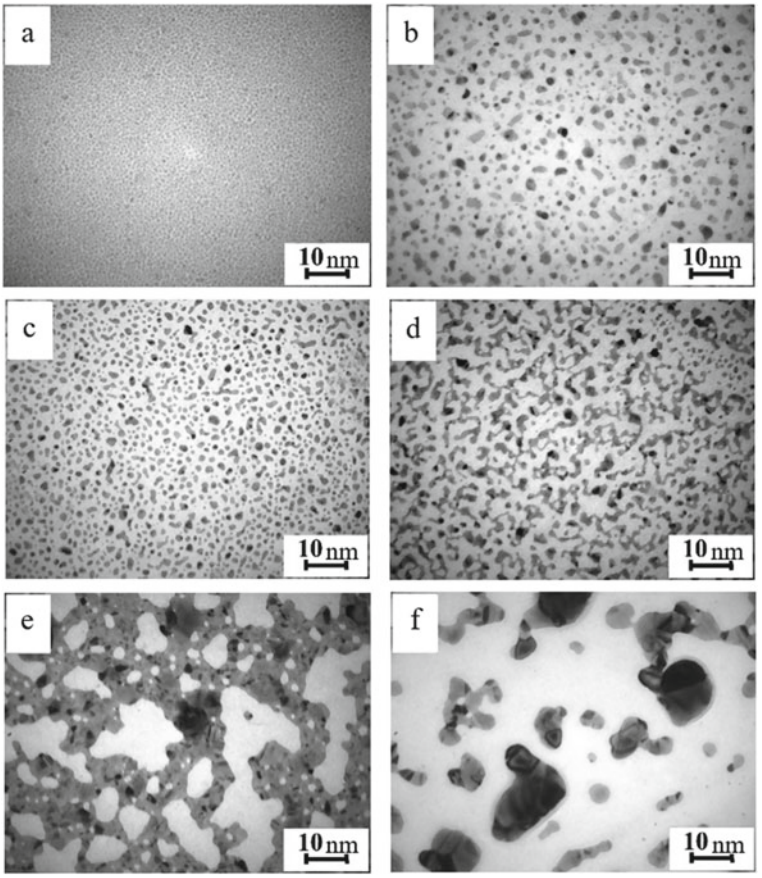

Fig. 8 Microstructure of unannealed (**a**) and annealed to 700 K (**b–f**) ultrathin NiCu alloy films of different thicknesses: d = 1 nm, C_{Cu} = 50.3 at.% (**a**, **b**); d = 2.5 nm, C_{Cu} = 36.7 at.% (**c**); d = 3.5 nm, C_{Cu} = 86.5 at.% (**d**); d = 6 nm, C_{Cu} = 90.5 at.% (**e**); d = 6.5 nm, C_{Cu} = 9.8 at.% (**f**)

along with this, there is also a significant decrease in their total number (Fig. 8b, c). At effective thicknesses d ≈ 3–4 nm, a characteristic «bridge» structure is formed in film alloys (Fig. 8d).

The most significant transformations during thermal stabilization annealing are experienced by films of approximately the same thickness d ≈ 6–6.5 nm, but with different component compositions. So, at high copper concentrations, the film becomes electrically continuous (see Fig. 8e), while at low copper concentrations (C_{Cu} = 9.8 at.%), the film remains island-like (Fig. 8f) with individual islands of complex shape, having sizes up to 20 nm. At the same time, crystals are visible inside the islands (even rather small ones), the shape, size, and number of which are not constant. Their appearance can be associated with the onset of recrystallization processes. The unification of the islands themselves into larger ones (Fig. 8f) obviously occurs according to the mechanism of «liquid-like» coalescence [32].

Features of the crystal structure of NiCu alloy films in a given range of thicknesses in a certain way affect the electrical properties (resistivity, TCR) of the samples under study.

With an increase in thickness (d > 10 nm), all the investigated alloy films in the freshly condensed state at T_s = 300 K become structurally continuous (Fig. 9a) and have an exclusively dispersed structure (average crystallite size L ~ 5 nm), which causes the angular expansion of the lines on electron diffraction patterns (see Fig. 6c). For NiCu films annealed to T = 700 K (Fig. 9b, c), the grain size increases to L ≈ kd, where k = 1–1.3.

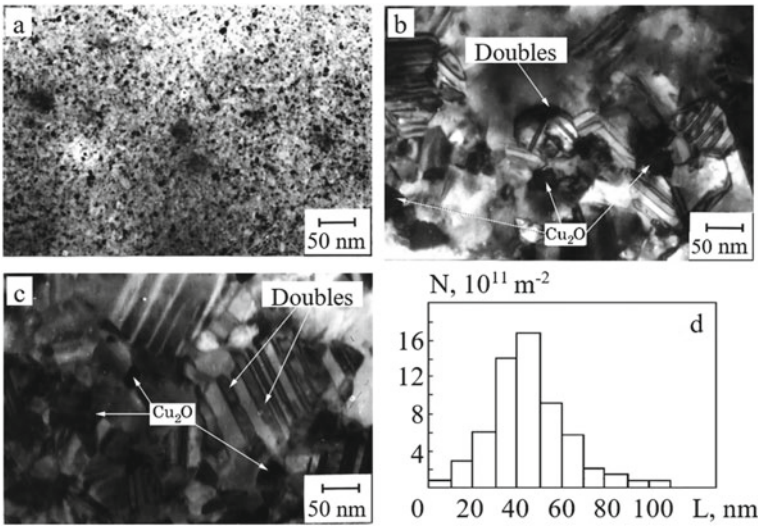

Fig. 9 Microstructure (**a**–**c**) and histogram (**d**) of unannealed (**a**) and annealed at 700 K (b-d) NiCu film alloys: d = 40 nm, C_{Cu} = 38 at.% (**a**, **b**, **d**); d = 80 nm, C_{Cu} = 60 at.% (**c**). Substrate-carbon film

As noted above, sometimes, at the first stages of annealing, electron microscopic images of NiCu film alloys show Cu_2O oxide crystallites in the form of translucent dark regions. Micrographs illustrating the processes of formation of Cu_2O and recrystallization of a film alloy with parallel polygonization (breaking of grains into individual subgrains by twins of thermal origin) are shown in Figs. 9. It should be noted that in the annealed samples, the average crystallite size before polygonization is 100–300 nm, which is much larger than in the original samples.

Influence of Temperature and Substrate on the Crystal Structure of NiCu Alloy Films

One of the main parameters that determine the process of crystallization of a film sample on a substrate is the substrate temperature T_s. Changing it leads to a change in a number of processes occurring simultaneously. Thus, with an increase in T_s, the mobility of condensed atoms migrating over the surface of the substrate increases, the desorption of adsorbed atoms of the deposited substance (as well as foreign particles and impurities) increases, the concentration of surface defects decreases, which leads to the formation of coarse-grained films with a more perfect structure, having an increased degree of texture (in the case of using oriented NaCl and KBr substrates).

To study the effect of substrate temperature on the crystal structure of NiCu alloy films, samples were deposited on (001) KBr substrates at various temperatures T_s at a rate of $\omega \approx 0.5$–1.5 nm/s. The nature of the influence of the substrate temperature on the crystal structure of the samples is shown in Fig. 10.

Films crystallized at room temperature are characterized by a fine-grained structure with an average crystallite size of ~5–10 nm (Fig. 10a). Such a crystal structure corresponds to a diffraction pattern in the form of slightly blurred rings (Fig. 10b), which indicates the small size of the crystals and their random orientation with respect to the substrate.

An increase in the substrate temperature to 373 K does not lead to a noticeable increase in the average grain size, as can be seen from Fig. 10c; however, the redistribution of the intensity of diffraction rings observed on the electron diffraction patterns (see Fig. 10d) may indicate the beginning of the oriented growth of some grains relative to the substrate.

A further increase in the substrate temperature during condensation to $T_s = 473$ K leads to the formation of a crystalline structure with grain sizes 50–70 nm (Fig. 10e). Simultaneously with the coarsening of crystallites, the number of oriented grains also increases, as evidenced by the contraction of the arches on the rings of electron diffraction patterns (see Fig. 10f).

In alloy films deposited on a substrate at a temperature of $T_s = 573$ K, a coarse-grained structure is observed with grain sizes reaching 70–100 nm (Fig. 10g). With a given crystal structure, an electron diffraction pattern is observed in the form of thin rings with point reflections of the corresponding (001) orientation placed on them (Fig. 10h). In addition, additional reflections are also observed on the electron

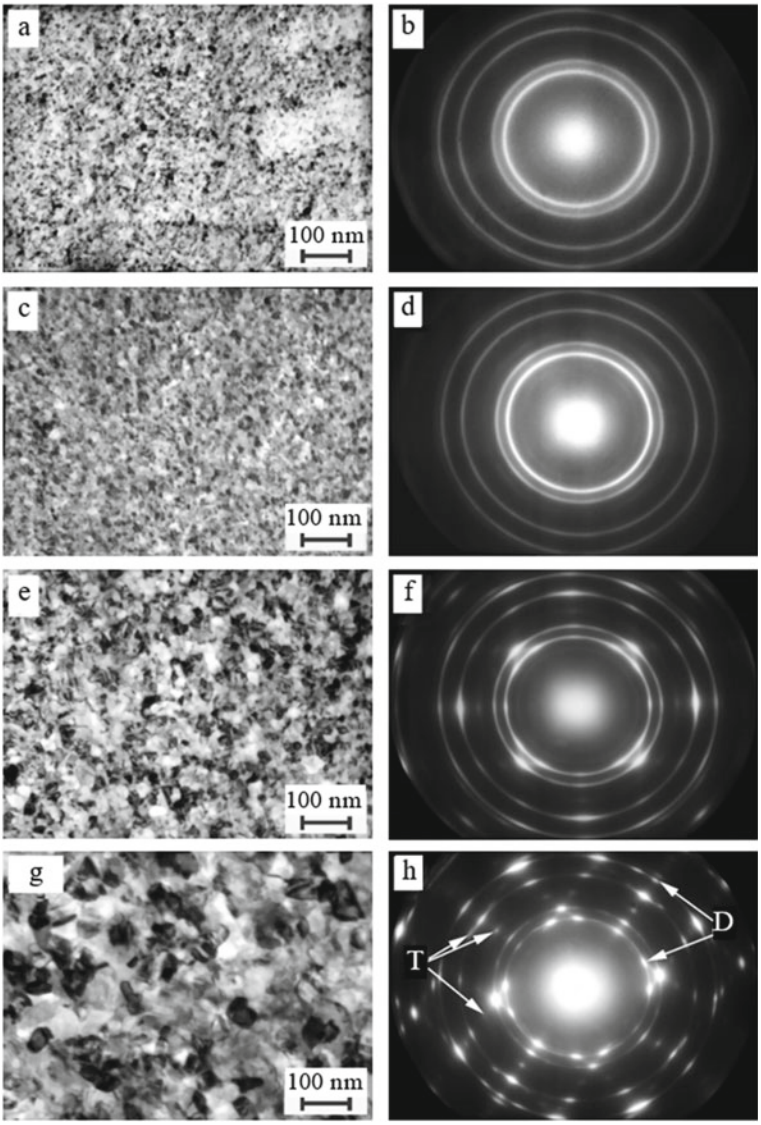

Fig. 10 Microstructure and corresponding electron diffraction patterns of NiCu alloy films (d = 40–60 nm, C_{Cu} = 22–28 at.%) deposited on (001) KBr cleavages at T_s = 293 K (**a**, **b**), T_s = 373 K (**c**, **d**), T_s = 473 K (**e**, **f**), T_s = 573 K (**g**, **h**)

diffraction patterns (marked D in Fig. 10h), which can be explained by the presence of doubles, the formation of which is a characteristic feature of thin films of many metals with an fcc lattice crystallized on alkali halides during thermal evaporation in vacuum (doubles are present on all {111} planes). The bands connecting the reflections (200) and (111) on the electron diffraction pattern (Fig. 10h) indicate the small size of the doubles.

Some dim additional reflections (marked T in Fig. 10h) can be explained by double diffraction (an electron beam diffracted from a matrix with orientation (001) hits the double and diffracts again, or vice versa). Their appearance occurs at some deviation from the exact orientation [100], i.e. with some film tilt. The oriented growth of the investigated thin films of NiCu alloys begins at the substrate temperature $T_s \approx$ 373 K. NiCu alloy films obtained by deposition on KBr (001) cleavages at different substrate temperatures were subjected to thermal stabilization annealing in vacuum together with the substrate up to 673 K. The annealing of films on a substrate at higher temperatures is impractical due to the strong sublimation of KBr, which can lead to the destruction of the film sample.

An analysis of the results obtained shows that the annealing of alloy films obtained at room temperature and $T_s = 373$ K leads to a significant increase in the size of crystallites up to 100 nm or more (Fig. 11a, c). The formation of doubles and an increase in the number of grains oriented parallel to the plane of the substrate are also observed (textural maxima in Fig. 11d).

For films obtained at substrate temperatures of 473 K and 573 K, upon annealing to 673 K, an increase in the crystallite size up to 200 nm is observed. Along with this, the appearance of new crystallites with sizes of 5–10 nm is also observed (Fig. 11e, g) due to the polygonization process. Additional reflections in the corresponding electron diffraction patterns (Fig. 11f, h) are due to both twinning and the presence of stacking fault tetrahedra (SFT in Fig. 11g).

5.2 NiCo Alloy Films

Some NiCo alloy films were obtained using the finite sample evaporation method. A series of bulk NiCo alloys of known composition was prepared for evaporation.

According to the data of the phase diagram (Fig. 4), for NiCo alloys at temperatures close to the melting point and in the liquid state, complete mutual solubility of the components is observed in the entire concentration range. In this case, the liquidus and solidus lines coincide, which excludes the possibility of alloy fractionation during melting.

In general, during the evaporation of binary alloys, the composition of the film differs from the composition of the initial material due to the fact that one of the components may have a high evaporation rate. The evaporation rate of the material at temperature T is determined by the formula [33]:

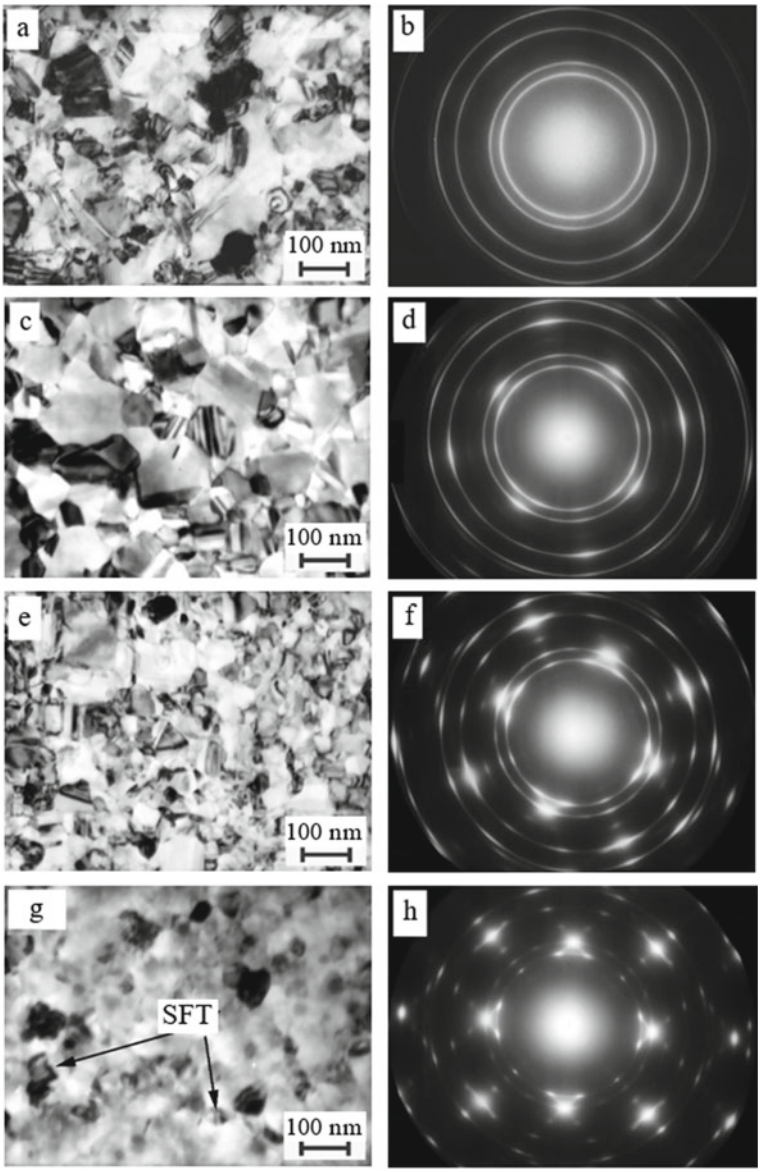

Fig. 11 Microstructure and corresponding electron diffraction patterns of NiCu alloy films annealed to 673 K (d = 40–60 nm, C_{Cu} = 22–28 at.%) deposited on (001) KBr cleavages at T_s = 293 K (**a**, **b**), T_s = 373 K (c, d), T_s = 473 K (**e**, **f**), T_s = 573 K (**g**, **h**)

$$v = kp\sqrt{\frac{M}{T}} = A_1 p, \tag{4}$$

where k is a constant; p is the vapor pressure; M is the molecular weight of the substance; T is the evaporation temperature.

When alloys are evaporated in a vacuum, the vapor pressure of each of the components above the melt is determined by the composition of the alloy and differs from the values for pure components. In the simplest case, the vapor pressure of component A (p_A) in the presence of component B (p_B) is determined by Raoult's law:

$$\frac{p_A - p_{AB}}{p_A} = C_B, \tag{5}$$

where C_B is the mole fraction of component B (the ratio of the number of moles of this component to the total number of moles of all components).

In [33], a method for calculating the fractionation of binary systems during the evaporation of final samples was proposed. Let at the initial moment of time in the evaporator there is a binary alloy with a mass content of the components m_{01} and m_{02}. During the time dt, taking into account the expression for the evaporation rate (4), the decrease in the mass of each of the components is

$$dm_A = -kp_{0A} f_A \sqrt{\frac{\mu_A}{T}} C_A(t)dt, \tag{6}$$

$$dm_B = -kp_{0B} f_B \sqrt{\frac{\mu B}{T}} C_B(t)dt, \tag{7}$$

where k is a constant depending on the choice of the system of units; p_{0A}, p_{0B} is saturation vapor pressure of pure components A and B of the alloy at temperature T; f_A, f_B areactivity coefficients of the components:

$$f_A = \frac{\alpha_A}{C_A}, \tag{8}$$

where $\alpha_A = \frac{p_{AB}}{p_A}$ is theactivity of component A (similarly for component B); $C_A(t)$, $C_B(t)$ are the atomic parts of the components; μ_A, μ_B are their molar masses. If Raoult's law is fulfilled (ideal melts), we have

$$1 - \frac{p_{AB}}{p_A} = C_B,$$

$$\alpha_A = \frac{p_{AB}}{p_A} = 1 - C_B = C_A, \tag{9}$$

whence $f_A = f_B = 1$.

According to the data of [15], the same saturation vapor pressures for Co and Ni are achieved at close temperatures (for example, $p_{Co} = 1.33$ Pa at T = 1790 K, p_{Ni} has the same value at T = 1800 K; a similar situation occurs for high pressures), so we can take $p_A = p_B$. In addition, the molar masses of Co and Ni are close ($\mu_{Co} =$ 58.9 g/mol, $\mu_{Ni} = 58.7$ g/mol), which means that for the mass parts of Co and Ni we obtain the ratio:

$$C_{Co} = \frac{C_{Co}\mu_{co}}{C_{Co}(\mu_{co} - \mu_{Ni}) + \mu_{Ni}} = \frac{58.9}{C_{Co}(58.9 - 58.7) + 58.7} C_{Co}$$
$$= \frac{58.9}{58.7 + 0.2C_{co}} C_{Co} \approx C_{Co}$$

Then

$$kp_{0A} f_A \sqrt{\frac{\mu A}{T}} \approx kp_{0B} f_B \sqrt{\frac{\mu B}{T}}.$$

As a result, the mass fraction of Co in the resulting alloy will be

$$c_{Co}{}' = \frac{dm_{Co}}{dm_{Co} + dm_{Ni}} = \frac{C_{Co}}{C_{Co} + C_{Ni}} = C_{Co} = c_{Co}. \quad (10)$$

Thus, under the condition that the Raoult law is satisfied, the concentration of the components in the film NiCo alloy should be the same as in the bulk sample, and the films should be homogeneous in chemical composition.

In accordance with the data of [16], bulk NiCo alloys with a Co content of up to 65–67 wt.% at room temperature form substitutional solid solutions with an fcc lattice over the entire temperature range of the solid state. For $C_{Co} > 75$ wt.% at 300 K, the solid solution has an hcp lattice based on α-Co; with an increase in temperature, an fcc lattice based on β-Co is formed (the temperatures of the direct and reverse hcp → fcc transitions depend on the concentration of the components). In the intermediate concentration range, a two-phase composition (fcc + hcp-tr.) is observed (Fig. 4).

The results of the analysis of electron diffraction patterns of films of the CoNi alloy with different concentrations of components (Fig. 12) show that patterns similar to massive alloys are observed for alloy films. For unannealed films with $C_{Co} \leq 70$ wt.% (Fig. 12a), the lines of only the fcc phase are recorded by electron diffraction. In this case, the diffraction maxima are quite wide, which indicates a small crystallite size. Annealing of the samples does not lead to a change in the phase composition of these films; only fcc-tr. NiCo (Fig. 12b–d). Thermal stabilization leads to a decrease in the width of the lines in the electron diffraction patterns and an increase in their intensity. The reason for this is the increase in grain size in the sample.

At a Co content of 75 wt.%, the films most likely have an fcc structure. The analysis of electron diffraction patterns in this case is difficult, since, due to the dispersion of the structure of the films, the lines in the electron diffraction patterns are quite wide, and the interplanar distances for the most intense lines of the fcc and hcp lattices are

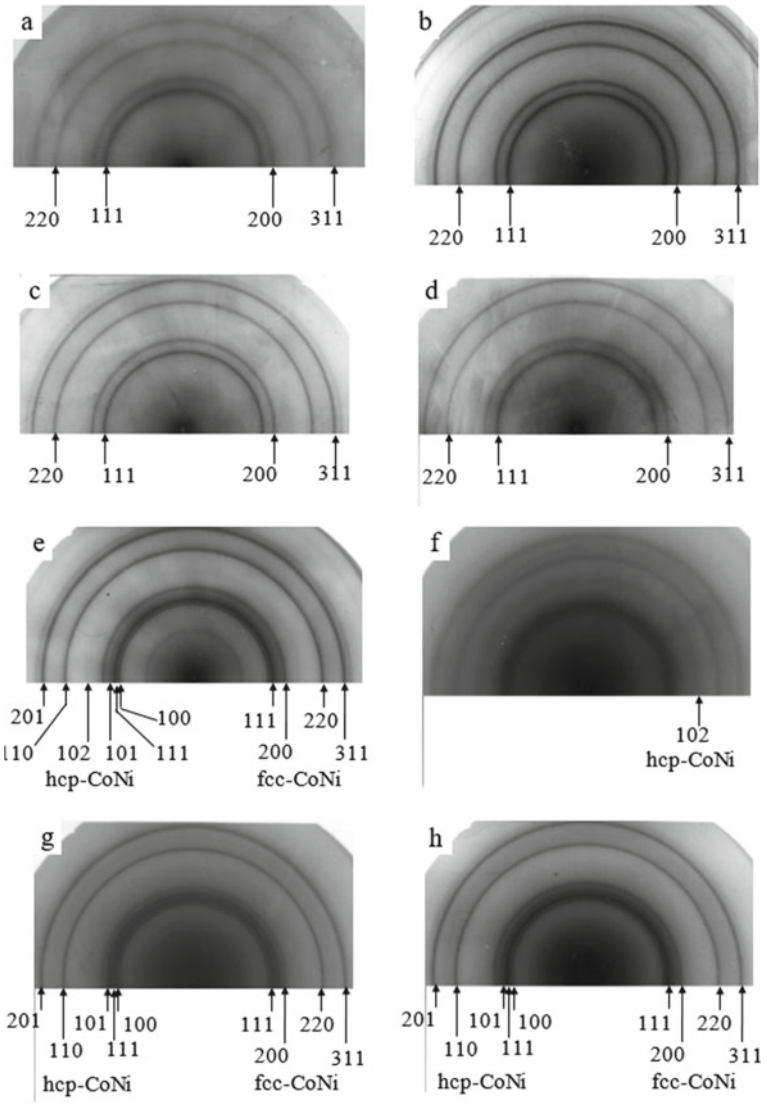

Fig. 12 Phase composition of unannealed (a, f) and annealed (b-e, g-h) NiCo films. Co content: **a**, **b** 10 wt.%; **c** 30 wt.%; **d** 70 wt.%; **e** 75 wt.%; **f**, **g** 80 wt.%; **h** 90 wt.%

almost the same. As a result, it is impossible to confidently separate the lines of each of the phases. Annealing to a temperature of 500–700 K leads to a decrease in the line width and the lines of both phases are fixed on the electron diffraction patterns (Fig. 12e), and the intensity of the lines of the fcc phase is higher. As is known [17], in a two-phase region, lines of both phases are observed in the diffraction pattern, when the composition of the phases is constant and corresponds to the boundaries

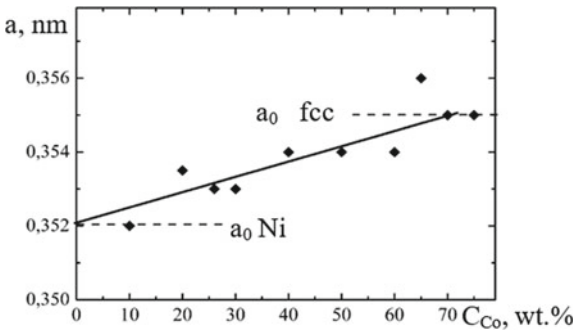

Fig. 13 Dependence of the fcc lattice parameter on the Co concentration for films of NiCo alloys

of the regions in the phase diagram. The lattice parameters of each of the phases also remain unchanged. A change in the concentration of the components causes only a change in the phase ratio, and, as a consequence, a change in the intensity of the lines. Thus, as the cobalt concentration increases, the intensity of the lines of the hcp lattice of the NiCo solid solution will gradually increase and, accordingly, the intensity of the lines of the fcc solid solution will decrease. Since the relative intensity of the phase lines is proportional to its volume (and, given the close values of the density of materials, and mass) fraction, the higher intensity of the fcc phase lines may indicate its higher content in the alloy of a given concentration. These reflections are confirmed by the presented electron diffraction patterns (Fig. 12).

Based on the results of studies of films of alloys with an fcc lattice, we built an experimental dependence of the lattice parameter on the concentration of Co (Fig. 13). It can be seen from the figure that an increase in the concentration of Co atoms leads to an increase in the fcc lattice parameter of the alloy according to a linear law, i.e. for films of fcc-NiCo alloys, Vegard's rule is observed.

For unannealed samples with CCo $\geq$ 80 wt.% (Fig. 12f), in full accordance with the state diagram of massive alloys, the electron diffraction lines of the hcp grating are observed. This can be confirmed by the presence of the (102) line, which is absent for the fcc lattice. As a result of annealing, a two-phase composition (fcc + hcp) is observed in these samples (Fig. 12g, h), while the intensity of the hcp lines is noticeably greater. Obviously, when the samples are heated to 700 K, a phase transition occurs in them with the formation of a high-temperature fcc phase, since the transition temperature is less than 700 K (with an increase in the Ni content in the alloys, the transition temperature decreases). However, despite the relatively slow cooling, the reverse transition does not completely pass, and a certain amount of the fcc phase remains in the sample. A possible reason for this is the size phase effect. According to the data of [34], the fcc phase can exist in small Co particles at temperatures below the end point of the reverse transition. Due to the rather significant size dispersion of crystallites in our samples (which is indicated by the data of electron microscopy studies), for that part of the crystallites, the sizes of which are much smaller than average, the fcc phase can remain stable, while in larger crystallites after cooling, an hcp phase is formed. According to electron diffraction data, the

lattice parameters of these phases are: for the fcc phase a = 0.355–0.357 nm; for hcp a = 0.248–0.252 nm, c = 0.410–0.432 nm, which is in good agreement with similar data for bulk alloys.

As noted earlier, at the initial stages of film formation, features of the structural state are observed, in particular, at small thicknesses, the films are structurally and electrically discontinuous (island). In connection with this, we carried out a study of the structure of ultrathin (d < 20 nm) NiCo films, the results of which are shown in Fig. 14. Since the condensation was carried out on a neutral non-oriented substrate (carbon film) at room temperature ($T_s \approx 300$ K < $2T_m/3$), the diffusion mobility of atoms on the substrate was hindered. As a result, in unannealed films, regardless of composition and thickness (Fig. 14a), almost the same structure was observed: islands of irregular shape with sizes less than 3 nm, and the gaps between them look like channels of approximately the same width (classical «labyrinth» structure [35]).

Annealing such films up to 700 K leads to a significant morphological change in their structure. With a small thickness (d ≈ 5–10 nm), a simple enlargement of the islands occurs due to coalescence (Fig. 14b). With a greater thickness d ≈ 15–20 nm (Fig. 14c–d) «bridges» appear between the islands, and a further increase in thickness (Fig. 14f) leads to the formation of electrically and then structurally continuous films. When the islands are enlarged, the crystal structure is also improved, which is manifested in the formation of islands with a clear cut (Fig. 14d, f).

An analysis of electron microscopic images shows that for unannealed films of the entire concentration range, a strongly fine-grained structure with a crystallite size of 1–2 nm is observed (Fig. 14a), which explains the reason for the significant width of the diffraction maxima. Crystallites do not have a clear cut, so the statistical processing of data regarding their size is difficult. The micrographs indicate the formation of a large number of small crystallization centers during the deposition process and their simultaneous growth.

We have made an attempt to check the manifestation of the phase size effect in films of this alloy. For ultrathin films with a thickness of d = 9 nm with a cobalt content of 80 wt.% (Fig. 14b), lines of both phases are observed on the electron diffraction patterns; however, the relative intensity of the lines of the fcc lattice is noticeably greater than that of the hcp lattice, in contrast to thicker continuous films (Fig. 14g). Since the intensity of the electron diffraction lines is proportional to the volume content of this phase, it is obvious that in island films, compared to thicker continuous films, the fraction of the fcc phase is larger than the fraction of the hcp phase.

The reason for this is the small size of crystallites (phase size effect). Unfortunately, this statement is only qualitative, since the electron diffraction reflections from ultrathin film alloys are extremely weak.

The results of electron microscopic studies of the crystal structure of solid film samples (d = 50–60 nm) are shown in Figs. 15.

Unannealed films (Fig. 15a) of all studied component concentrations have approximately the same structure—small crystallites 5–10 nm in size without a clear cut. In the process of thermal stabilization, an increase in the size of crystallites is observed due to recrystallization processes (Fig. 15b–d).

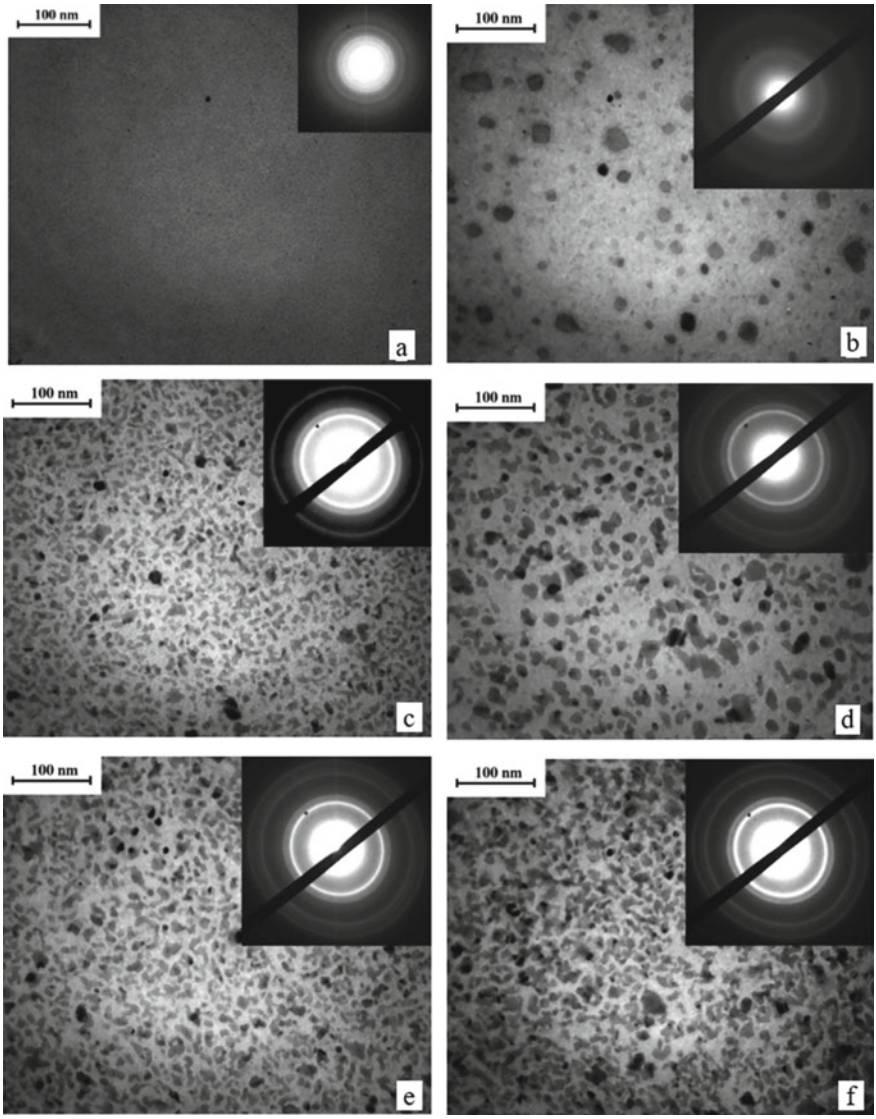

Fig. 14 Morphology of unannealed (**a**) and annealed to 700 K (**b–f**) ultrathin NiCo alloy films: **a** d = 20 nm, C_{Co} = 20%; **b** d = 9 nm, C_{Co} = 80%; **c d** = 9 nm, C_{Co} = 10%; **d** d = 10 nm, C_{Co} = 30%; **e** d = 15 nm, C_{Co} = 70%; **f** d = 20 nm, C_{Co} = 50%

For some of the crystallites, a clear faceting and the presence of stacking faults (most likely of growth origin) are observed. To estimate the size of crystallites in the film plane, statistical processing of micrographs was carried out with the construction of histograms (Fig. 16). The average grain sizes determined on their basis have a value of 110–200 nm and show a slight tendency to coarsen with increasing Co content.

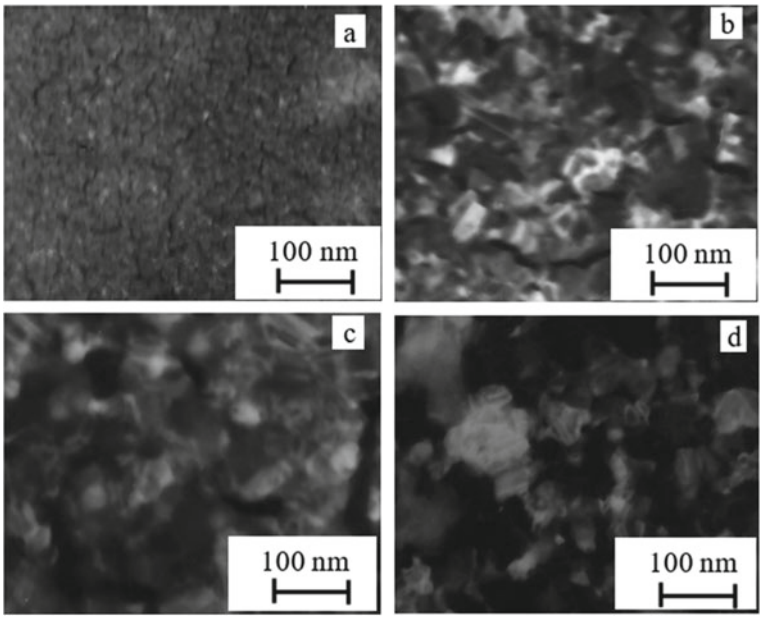

Fig. 15 Microstructure of NiCo film alloys with a thickness of d = 60 nm: **a** typical structure of an unannealed film (C_{Co} = 70 wt.%); **b–d** film structure after thermal stabilization (**b** C_{Co} = 10 wt.%; **c** C_{Co} = 50 wt.%; **d** C_{Co} = 90 wt.%)

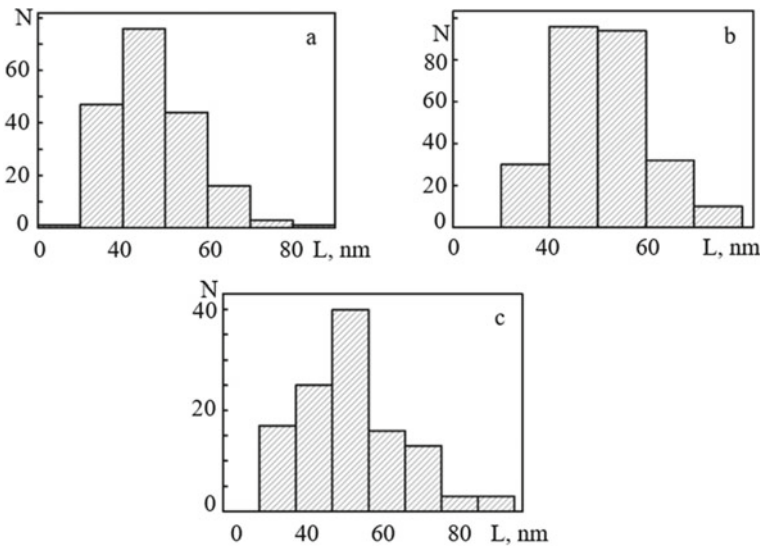

Fig. 16 Histograms for determining the average sizes of crystallites in the film plane: **a** C_{Co} = 50 wt.%; **b** C_{Co} = 70 wt.%; **c** C_{Co} = 90 wt.% (d = 60 nm)

Electron microscopic investigations make it possible to determine the sizes of crystallites in the film plane. We have made an attempt to estimate the sizes of crystallites in the direction of the normal to the film plane (to estimate the «height» of crystallites) by determining the sizes of coherent scattering regions (CSR). Determining the size of the CSR in the direction of the normal to the film is possible on the basis of an analysis of the broadening of the profiles of diffraction lines in the electron diffraction patterns.

The limited size of the CSR leads to an increase in the line width, and the line broadening is inversely proportional to the size of crystallites or blocks. The integral width β of the line is determined by the Selyakov-Scherer formula [36]

$$\beta = \frac{m\lambda}{L_{\perp} cos\theta}, \tag{11}$$

where m is a coefficient depending on the shape of crystallites, m = 0.98–1.38 (m ≈ 1 can be considered); λ is the de Broglie wavelength of electrons; $L_{\perp}$ is the average size of crystallites in the direction of the beam; θ is the Bragg angle.

In the electron diffraction analysis, the angles θ do not exceed 5°; therefore, cosθ ≈ 1 can be taken with sufficient accuracy. As a result, the crystallite size can be estimated from the formula:

$$\beta = \frac{m\lambda}{L_{\perp} \cos\theta}, \tag{12}$$

where $\beta = \frac{1}{f(0)} \int f(2\theta) d(2\theta)$.

The value of β represents the integral width of the peak, the shape of which is described by the function f(2θ). Since the integral in the numerator of this expression determines the area of the curve under the peak, and the denominator determines the maximum height of the peak, the value of β is the width of a rectangle of the same area and the same height as the peak.

It should be noted that the broadening of diffraction lines can also occur for other reasons. Among them, instrumental broadening, which is determined by the shooting conditions, plays a significant role. The instrumental broadening can be taken into account by shooting a reference sample, which is a coarse-grained film sample free from microstresses (we used the line broadening of the annealed Al reference sample).

Line broadening is also possible due to the existence of microstresses in the sample and a significant number of randomly located dislocations. For these cases, we have

$$\beta = 4\varepsilon tg\theta,$$

where $\varepsilon = \frac{\Delta d}{d_0}$ is therelative change in interplanar spacing (microstrain); Δd_m is thevolume-averaged maximum change in interplanar spacing; d_0 are interplanar distances in an ideal crystal. However, due to the small diffraction angles, the contribution of these factors to the total broadening is insignificant. Figure 17 shows the

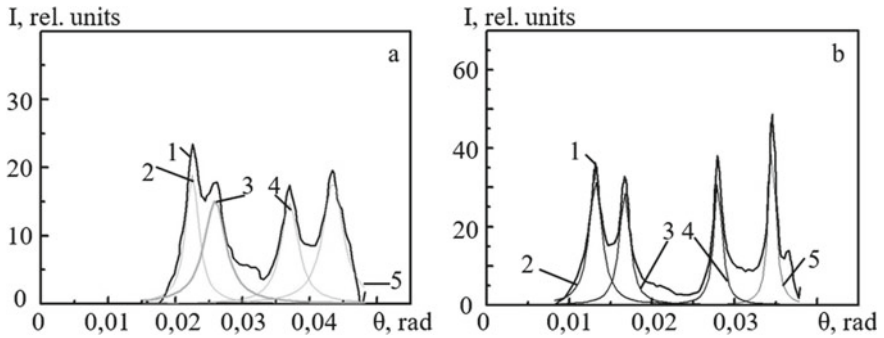

Fig. 17 Angular intensity distribution of diffraction maxima for NiCo alloy film d = 70 nm with C_{Co} = 10 wt.%: **a** unannealed; **b** annealed film. 1—experimental intensity distribution, 2-5—approximation of peaks

experimental (curves 1) used by us for the angular dependences of the intensity distribution of diffraction lines on the electron diffraction patterns and the approximation lines (curves 2–5) obtained using the Microcal Origin data processing package. When calculating the magnitude of the broadening, the approximation of the peak shape by the Cauchy function was used.

The computer selection of the function parameters made it possible to describe the peaks obtained after the background value was taken into account as accurately as possible. The half-width of the peak, expressed in angular units, was taken as the value of physical broadening. The values obtained for unannealed films (5–10 nm) coincide in order of magnitude with the data of electron microscopic studies, which indicates an approximately equiaxed shape of crystallites. In addition, these data show that the films are in a nanocrystalline rather than amorphous state. As a result of heat treatment, an increase in the size of crystallites is observed both in the film plane and in the direction normal to the sample. The values of grain sizes determined from line broadening have a value of the order of 20–25 nm. Thus, the annealed NiCo alloy films consist of crystallites whose dimensions in the substrate plane are 100–200 nm, and in the direction perpendicular to the substrate plane, they are 5–10 times smaller, i.e. crystallites have a significant unevenness.

We also note the features of the structural-phase state of NiCo film alloys obtained by simultaneous condensation of Co and Ni during evaporation from independent sources (electron-beam guns). In general terms, the structure of alloy films obtained by this method is identical to the structure of alloys obtained by evaporation of sample portions—unannealed films consist of small crystallites 5–10 nm in size; as a result of annealing, an increase in crystallite size up to 50–100 nm is observed, depending on the annealing temperature. However, the phase composition of such films has a number of significant differences.

In Figs. 18 and 19, for example, the microstructure of NiCo films with a thickness of d = 50 nm with a sharply different concentration of components—14 wt.% Co (Fig. 18) and 73 wt.% Co (Fig. 19) before and after annealing at T = 1300 K.

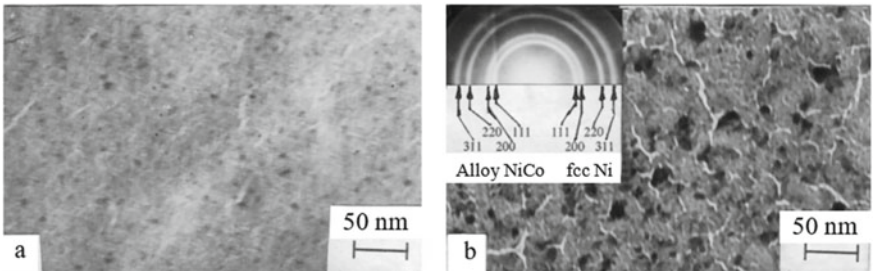

Fig. 18 Microstructure of NiCo alloy films (C_{Co} = 14 wt.%, d = 50 nm). Temperature: **a** 300 K; **b** 1300 K

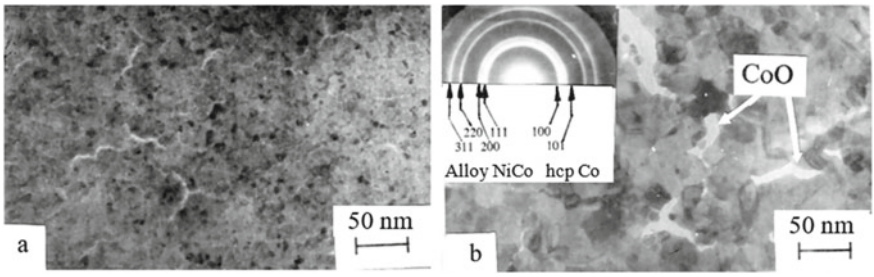

Fig. 19 Microstructure of NiCo alloy films (C_{Co} = 73 wt.%, d = 50 nm). Temperature: **a** 300 K; **b** 1300 K

The initial state (Figs. 18a, 19a) of both film samples is almost the same—small crystallites 5–10 nm in size, which does not allow reliable identification of their phase composition using electron diffraction patterns (significant width of diffraction maxima). After annealing the samples (Figs. 18b, 19b), an almost identical increase in the size of crystallites is observed as a result of recrystallization processes, while the phase composition (electron diffraction patterns in the insets) differs significantly.

In both cases (both at low and high cobalt concentrations), the films exhibit a two-phase composition: (fcc-Ni) + (fcc-NiCo) and (fcc-NiCo) + (hcp-Co), respectively, although, according to the state diagram of a massive alloy (Fig. 4) at low concentrations of Co, only the fcc-NiCo alloy is formed.

The reason for these differences, most likely, is that the formation of a NiCo solid solution with simultaneous condensation of Co and Ni on the substrates at $T_s = 300$ K does not occur to the end (nonequilibrium process), so that even high-temperature (T = 1300 K) annealing does not allow completely relax this disequilibrium.

It should also be noted that the micrographs of samples with $C_{Co} > 50$ wt.% show stacking faults (which appeared during annealing) and characteristic extinction contours (Fig. 19b). Here, the same feature occurs that is also observed in Co films: when the crystallite size is less than 10 nm, the formation of stacking faults in them is difficult, which is associated with a high energy barrier to the displacement of Shockley dislocations (it is known that the growth of a stacking fault begins on the

{111} fcc lattices as a result of the splitting of full dislocations into two partial ones). High-temperature recrystallization processes, leading to an increase in grains, cause only a slight decrease in the energy of partial dislocation nucleation.

When film alloys are annealed to 700 K, the formation of CoO and NiO oxides is practically not observed in them. In films that have been annealed to a temperature of T = 1300 K, in parallel with an increase in the size of crystallites, the formation of fine-grained oxide CoO is observed in samples with $C_{Co} > 15$ wt.% (Fig. 4b).

5.3 NiFe Film Alloys

To obtain films of NiFe alloys, we used the method of evaporating final portions of the finished NiFe alloy known as permalloy 50N.

The NiFe system obeys Raoult's law almost perfectly. It is also characterized by complete mutual solubility of the components in the solid state at high temperatures and in the liquid state (Fig. 5). In this case, for iron, the temperature at which its saturated vapor pressure becomes equal to the nickel saturated vapor pressure is approximately 50 K lower than the nickel temperature [15]. The evaporation rate of iron under such conditions becomes much higher than that of nickel.

Thus, during the evaporation of finished alloys, the fractionation of the composition of the films is possible (change in the composition along the thickness), and at the initial moments of evaporation, the films will be enriched in iron. Such conclusions are confirmed by the data of [37].

According to the literature data [38], in bulk samples of the NiFe alloy, a compound with an fcc lattice (taenite) is observed with a lattice parameter varying from 0.3524 nm (pure Ni) to 0.3596 nm ($C_{Ni} = 39\%$). In particular, the composition with $C_{Ni} = 49\%$ corresponds to the value of the lattice parameter a = 0.3586 nm. The study of the phase composition of the films by electron diffraction showed that in all films there is an fcc phase with a lattice parameter a = 0.359–0.361 nm (Fig. 20, inset).

Thus, in film samples (compared to bulk samples), some increase in the lattice parameter is observed. It should be noted that the electron diffraction patterns of the NiFe alloy films also show a number of lines that may belong to the NiFe intermetallic phase with the P4/mmm space group. Unannealed films have a fine-grained structure (Fig. 20a), their annealing leads to an increase in grain size; however, grain sizes do not exceed 50 nm (Fig. 20b).

6 Conclusions

– The formation of the fcc NiCu alloy occurs on the substrate directly in the process of simultaneous condensation of the components in the entire thickness range; for structurally continuous annealed films, depending on the concentration of the

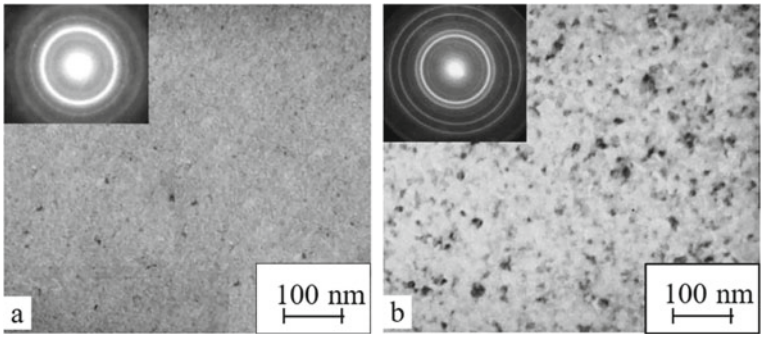

Fig. 20 Microstructure of NiFe alloy films (d = 36 nm) in the (**a**) unannealed and (**b**) annealed states. $T_s = 300$ K

components, the crystal lattice parameter is a = 0.353–0.362 nm in accordance with Vegard's rule;

- In films of NiCu alloys with effective thicknesses d < 10 nm, obtained on amorphous substrates at a temperature of T = 300 K, an island structure is observed with an average island size of 1.5–2 nm (unannealed samples) and up to 20 nm (annealed samples) depending on the effective thickness;
- Films of NiCu alloys with a thickness of d > 15–20 nm, obtained both on oriented ((001) KBr or NaCl) and non-oriented (carbon films) substrates at T = 300 K, have a fine-grained structure with an average crystallite size 5–10 nm; annealing to 700 K or condensation on a substrate heated to T_s = 400–600 K leads to an increase in the crystallite size to 50–100 nm; simultaneously with the coarsening of crystallites, the number of oriented grains also increases;
- In NiCo film alloys with a thickness of d < 15 nm, obtained on amorphous substrates at T = 300 K, an island structure is observed with an average island size of 1–2 nm in unannealed and 20–25 nm in annealed films, depending on the effective;
- Unannealed and annealed NiCo alloy films at $C_{Co} < 70$ wt.% have an fcc structure, annealed films with $C_{Co} \geq 80$ wt.% have a two-phase composition (fcc + hcp)-solid solution NiCo;
- The change in the lattice parameter of fcc-NiCo films with increasing C_{Co} is described by the Vegard rule;
- Unannealed film samples of NiCo alloys have a fine-grained structure with a crystallite size of 5–10 nm; as a result of annealing to T = 700 K, an increase in the average crystallite size in the film plane to 40–60 nm is observed;
- In unannealed films of NiCo alloys, crystallites have an equiaxed shape; after annealing in the direction normal to the film plane, their size is ~ 25 nm;
- For NiCo alloy films obtained by evaporation of Co and Ni from two independent sources, a two-phase composition is observed (fcc-Ni) + (fcc-NiCo) or (fcc-NiCo) + (hcp-Co);

– $Ni_{50}Fe_{50}$ alloy films have an fcc lattice with a = 0.359–0.361 nm; unannealed films have a fine-grained structure; annealing leads to an increase in grain size up to 50 nm.

References

1. Soni, V.K., Sanyal, S., Sinha, S.K.: Phase evolution and mechanical properties of novel $FeCoNiCuMo_x$ high entropy alloys. Vacuum **174**, 109173 (2020)
2. Hua, X., Li, J., Liu, H., Yang, Z., Liu, S.F.: Preparation of Cu_2Se thin films by vacuum evaporation and hot-pressing. Vacuum **185**, 109947 (2021)
3. Li, G., Song, G., Wang, N.: Influence of Cu content on the phase composition and thermoelectric properties of deposited Cu–Se films. Surfaces and Interfaces, p. 101651 (2022)
4. Pylypenko, O.V., Pazukha, I.M., Ovrutskyi, A.S., Odnodvorets, L.V.: Electrophysical and magnetoresistive properties of thin film alloy $Ni_{80}Fe_{20}$. J. Nano Electron. Phys. **8**(3), 03022 (2016)
5. Bereznyak, Y., Odnodvorets, L., Poduremne, D., Protsenko, I., Shabelnyk, Y.: High-entropy film alloys: electrophysical and magnetoresistive properties. Springer Proc. Phys. **210**, 17–24 (2018)
6. Shkurdoda, Y.O., Chomous, A.M., Shabelnyk, Y.M., Loboda, V.B., Khursenko, S.M.: Method of production and structural-phase state of medium-entropy Equiatomic FeNiCoCu film alloy. Proceedings of the IEEE 10th International Conference on Nanomaterials: Applications and Properties, p. 9309616 (2020)
7. Saltykov, D.I., Protsenko, S.I., Pazukha, I.M., Shkurdoda, Y.O.: Concentration and heat treatment effects on magnetoresistive properties of three-layer film systems based on Fe_xCo_{100-x} and Cu. Thin Solid Films **716**, 138422 (2020)
8. Bezdidko, O.V., Nepijko, S.A., Shkurdoda, Y.O., Shabelnyk, Y.M.: Structure and Magnetoresistive properties of three-layer films $Co_{(1-x)}Cr_x$/Cu/Co. J. Nano Electron. Phys. **13**(3), 1–4 (2021)
9. Loboda, V.B., Kolomiets, V.M., Khursenko, S.M., Shkurdoda, Y.O.: The electrical conductivity of the three-layer polycrystalline films Co/Ag(Cu)/Fe in the conditions of atoms interdiffusion. J. Nano Electron. Phys. **6**(1), 04032 (2014)
10. Loboda, V.B., Shkurdoda, Yu.O., Kravchenko, V.O., Khursenko, S.M., Kolomiets, V.M.: Structure and magnetoresistive properties of polycrystalline Co/Cu/Co films. Metallofiz. Noveishie Tekhnol. **33**(2), 161–169 (2011)
11. Loboda, V.B., Kolomiets, V.M., Shkurdoda, Yu.O., Kravchenko, V.O., Dekhtyaruk, L.V.: Structure and magnetoresistive properties of nanocrystalline film systems based on Co, Fe, Ag, and Cu. Metallofiz. Noveishie Tekhnol. **34**(8), 1043–1055 (2012)
12. Pogrebnjak, A.D., Lebed, A.G., Ivanov, Yu.F.: Modification of single crystal stainless steel structure (Fe–Cr–Ni–Mn) by high-power ion beam. Vacuum **63**(4), 483–486 (2001)
13. Pogrebnjak, A.D., Shablya, V.T., Sviridenko, N.V., Valyaev, A.N., Plotnikov, S.V., Kylyshkanov, M.K.: Study of deformation states in metals exposed to intense-pulsed-ion beams (IPIB). Surf. Coat. Technol. **111**(1), 46–50 (1999)
14. Pogrebnjak, A.D., Yakushchenko, I.V., Abadias, G., Chartier, P., Bondar, O.V., Beresnev, V.M. Takeda, Y., Sobol, O.V., Oyoshi, K., Andreyev, A.A., Mukushev, B.A.: The effect of the deposition parameters of nitrides of high-entropy alloys (TiZrHfVNb)N on their structure, composition, mechanical and tribological properties. J. Superhard Mater. **35**(6), 356–368 (2013)
15. Meissel, L., Gleng, R.: Thin Film Technology: Handbook. Moscow: Sov. Radio, Vol. 2, 768 p. (in Russian) (1977)

16. Ganina, N.I., Zakharov, A.M., Olenichev, V.G.: Diagrams of the State of Metallic Systems. Moscow: VINITI, Vol. 32, 626 p. (in Russian) (1988)
17. Lyakishev, N.P.: State Diagrams of Binary Metallic Systems: Handbook. Moscow: Машиностроение, 1996, Vol. 2, 1024 p. (in Russian) (1997)
18. Kikoin, I.K.: Tables of Physical Quantities. Handbook. Moscow: Atomizdat, 1008 p. (in Russian) (1976)
19. Nepiyko, S.A.: Physical Properties of Small Metal Particles. Kyiv: Naukova dumka, (in Russian) (1985)
20. Bar'yakhtar, V.G.: Solid State Physics: Encyclopedic Dictionary. Kyiv: Naukova dumka, 656 p. (in Russian) (1996)
21. Pushin, V.G., Blinov, S.G., Yurchenko, L.I.: Investigation of the microstructure of cobalt-nickel alloys metastable with respect to fcc-hcp martensitic transformation. Fizika Metallov i Metallovedeniye **75**(3), 96–109. (in Russian) (1993)
22. Langvagen, S.E., Lyubashevsky, O.P., Chizhov, P.E.: Magnetic properties of small particles of Fe–Ni alloys. Fizika Metallov i Metallovedeniye **9**, 69–73 (1991). (in Russian)
23. Komnik, Yu.F.: Physics of Metal Films. Dimensional and Structural Effects. Moscow: Atomizdat, 264 p. (in Russian) (1979)
24. Gladkikh, N.T.: Surface Phenomena and Phase Transformations in Condensed Films. Khar'kov: KHNU im. V.N. Karazina, 276 p. (in Russian) (2004)
25. Kukushkin, S.A., Osipov, A.V.: Processes of condensation of thin films. Uspekhi fizicheskikh nauk **168**(10), 1083–1116. (in Russian) (1998)
26. Protsenko, I.Yu., Saenko, V.A.: Thin Metal Slabs (technology and power). Sumi: SumDU, 187 p. (in Ukrainian) (2002)
27. Loboda, V.B., Saltykova, A.I., Khursenko, S.N.: Physical properties of thin nanocrystalline metal films: Book 1. Crystal structure, phase and elemental composition of films. Saarbrucken: LAP LAMBERT Academic Publishing, 113 p. (in Russian) (2014)
28. Loboda, V.B., Kravchenko, V.O., Shkurdoda, Yu.O. et al.: "Structure, electrical conductivity and galvanomagnetic power of thin melts of $Fe_{0.5}$–$Ni_{0.5}$ alloy", Visnyk SumDU. Seriya: Fizyka, matematyka, mekhanika **8**(67), 115–123. (in Ukrainian) (2004)
29. Goldshmidt, H.J.: Interstitial Alloys. Moscow: Mir, 424 p. (in Russian) (1971)
30. Semiletov, S.A., Zavyalova, A.A., Imamov, R.M.: About anomalous crystal structures in thin films of transition and rare-earth metals. Izvestiya AN SSSR **41**(11), 2230–2237. (in Russian) (1972)
31. Morokhov, I.D., Trusov, L.I., Chizhik, S.P.: Ultrafine Metallic Medium. Moscow: Atomizdat, 264 p. (in Russian) (1977)
32. Trusov, L.I., Kholmyansky, V.A.: Island Metal Films. Moscow: Metallurgiya, 320 p. (in Russian) (1973)
33. Kravchenko, V.A., Loboda, V.B., Protsenko, I.Yu. et al.: Structure and electrophysical properties of Ni–Co alloy films within 300–1300 K temperature range. Funct. Mater. **6**(5), 892–895 (1999)
34. Kuzmenko, A.I., Prokofiev, T.A., Protsenko, I.E. et al.: Phase diagram of the fcc-hp transition in small particles of cobalt. Izvestiya AN SSSR, №8, pp. 1590–1592. (in Russian) (1986)

35. Palatnik, L.S., Fuchs, M.Ya., Kosevich, V.M.: Formation Mechanism and Substructure of Condensed Films. Moscow: Nauka, 318 p. (in Russian) (1972)
36. Umansky, Ya.S., Skakov, Yu.A., Ivanov, A.N. et al.: Crystallography, X-ray Diffraction and Electron Microscopy. Moscow: Metallurgiya, 632 p. (in Russian) (1982)
37. Kostrzhitsky, A.I., Karpov, V.F., Kabanchenko, M.P., Solovieva, O.N.: Operator's Handbook for Vacuum Coating Plants. Moscow: Mashinostroyeniye, 176 p. (in Russian) (1991)
38. Maurice, F., Meny, L., Tixier, R.: Microanalysis and Scanning Electron Microscopy. Moscow: Metallurgiya, 392 p. (in Russian) (1985)